Journal of Hydroscience and Hydraulic Engineering
Vol.12, No.2, November, 1994, 1-16

FLOW CHARACTERISTICS AND ENTRAINMENT OF TWO-DIMENSIONAL STARTING PLUMES TRAVELING DOWNSLOPE

BY

Juichiro Akiyama, Masaru Ura, and Koichi Sakamoto

Department of Civil Engineering, School of Engineering
Kyushu Institute of Technology, Kitakyushu 804, Japan

SYNOPSIS

The flow characteristics of a miscible, two-dimensional starting plume traveling downslope have been investigated in the laboratory. A series of experiments was conducted to quantify a number of important flow properties. It is found from the application of a large volume of present experimental data that flow properties such as the dimensionless front propagation speed, the spatial growth rate, the rate of entrainment, as well as other flow characteristics, are at most functions of bottom slope angle θ for the range of θ=5~90° .The results of the study provide not only an understanding of the fundamental flow characteristics, but also the ability to develope an analytical or hybrid model for the phenomenon.

INTRODUCTION

When dense fluid is introduced into a less dense environment, it spreads under the action of buoyancy force and often travels down an incline. The flow of this form is referred to as a "gravity current". Examples of this in the atmosphere include pyroclastic flows, sea-breeze fronts, powder snow avalanches, and accidental release of dense industrial gases. Examples found in aquatic environments include spreading dense contarminated water, direct inflow of turbid water from a river to a lake, and marine turbidity currents resulting from landslides.

Differences in density may be caused by dissolved substances, temperature differences, or suspended material. A gravity current generated by conservative matter is called a "conservative gravity current", characterized as a flow whose initial buoyancy flux is maintained throughout the current. Conversely, a gravity current generated by nonconservative matter, such as suspended sediments, is called a "nonconservative gravity current". A gravity current over a sloping boundary can be in the form of either a "starting plume" or a "thermal", depending on whether the source is continuous or instantaneous. An inclined starting plume consists of an unsteady frontal zone characterized by a distinct raised-head structure, followed by an about-steady thinner flow. This unsteady head part of the flow is called the "front part" and downstream flow is known as the "body part". In contrast, the thermal consists only of a head structure without a distinct body part.

Among various forms of gravity currents, the present experimental study is concerned with the flow characteristics of conservative, two-dimensional, inclined starting plumes.A great deal of experimental study has been devoted to the determination of gross properties of flow, including geometry, propagation speed, and flow thickness of the front part. As a result, some useful information on the motion of inclined starting plumes has been quantified by Akiyama & Ura(2), Altinakar *et al.*(5), Britter & Linden(6), Hadano(7), Hopfinger & Tochon-Danguy(8),

Fukuoka *et al.*(9), Luthi(12), Middleton(14), Simpson & Britter(16), Wood(17) and others. Akiyama(4) concisely reviewed research on plumes and thermals conducted in Japan. Among these studies, Britter & Linden's study deserves special attention. Britter & Linden(6) examined some of the flow characteristics under a wide range of bottom slope angles(θ=5~90°) with the use of their own experimental data as well as existing data, while earlier studies addressed only limited parts of the parameter range. Altinakar *et al.*(5) attempted to encompass the investigation by Simpson & Britter(16), who studied the horizontal case(θ=0°), and the cases examined by Britter & Linden(6); Altinakar *et al.* investigated cases on inclines of less than 5° .

However, the data presented by both Britter & Linden and Altinakar *et al.* show a considerable scatter for all slopes, and uncertainty exists with regard to flow properties. This is not merely the result of experimental errors, but is mainly due to the fact that flow properties of the front part oscillate strongly from an intermittent loss of buoyancy, caused by large breaking eddies (billows), to the wake of the front part. This phenomenon is inherent in inclined starting plumes.

In the present study, a series of experiments was conducted on the spreading of a two-dimensional inclined starting plume produced by a continuous source of saline water. Such averaged flow properties as the front propagation speed, the geometry of the front, the entrainment coefficient, and other flow characteristics of starting plumes on inclines of slope angles ranging from 5° to 90° are quantified using a large volume of experimental data.

EXPERIMENT

The motion of an inclined starting plume is illustrated in Fig.1 along with the coordinate system and the notations to be used. A series of saline inclined plume experiments was conducted using two experimental facilities; a small glass wall flume (2.0m L, 0.36m D,0.22m W) for steeper slopes (θ=45° , 60° , 90°) and a large glass wall flume (10.0m L, 1.0m D, 0.205m W) for milder slopes (θ=5° , 5.17° , 8.13° , 10° , 20°). Experimental conditions are listed in Table 1.

The tank was filled with fresh water to a constant depth. From an elevated constant head tank, a constant discharge q_0 with buoyancy force $B_0(=\varepsilon_0 g)$ of dense saline water marked with a green fluorescent dye was quickly introduced into the flume at the upstream end and allowed to form an inclined starting plume, where ε=relative density difference $(=(\rho-\rho_a)/\rho_a)$.

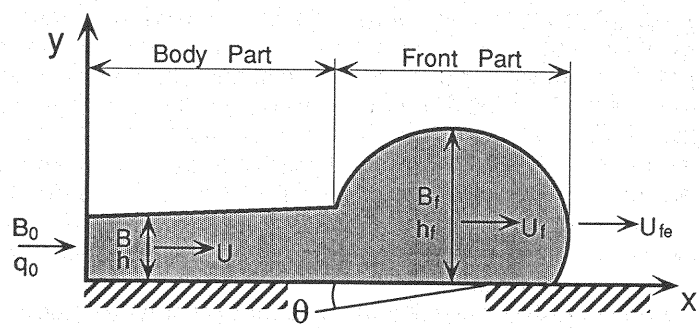

Fig.1 Definition Sketch of an Inclined Starting Plume.

In all cases, a flow visualization technique by use of a VTR camera was employed to quantify such gross properties of the flow as the front propagation speed U_{fe}, the geometry of the front part, and the layer thickness h of the body part. Only in the case of θ=5.17° and 8.13° , such local flow properties as the vertical velocity profiles of the body part u as well as the front part u_f and the density profiles of the body part ρ as well as the front part ρ_f were measured.

Local velocity was continuously recorded with three 3.0 mm diameter micro current meters (Shinozuka, Model SV-33W) with a measuring range of 2.5 to 100 cm/s. The signal was recorded on a strip-chart recorder. The current meters were placed parallel to the channel bottom, keeping the same distance from it. The lowest measurement point of 0.5 cm from the channel bottom was selected, and from this point three current meters were moved upward normal to the channel bottom. Zero velocity points at the upper interface of the flow were estimated from the displacement of dye lines produced by dropping small crystals of potassium permanganate from the water surface. Repeating experiments under the same conditions, vertical velocity distributions at different sections were determined.

Vertical density profiles were obtained using three sampling devices simultaneously. Each sampling device consisted of a rake of ten point samplers made of 1.0mm diameter brass tubing, jointed with a plastic pipe. As a steep density gradient is expected at the vicinity of the channel bottom, the lowest sampling point was set as close to the bottom as possible, and a point 1.0mm above the bottom was chosen. Particular care was taken for installing these samplers at the same elevation from the channel bottom, keeping required horizontal distance between sampling devices. An attempt was made to keep the amount of sampled water constant (10 cc). Assuming repeatability of experiments, experiments for velocity measurements by current meters, for density measurements by sampling devices, and experiments for gross flow properties using a VTR camera were conducted separately under the same experimental conditions. This was done to circumvent undesirable disturbances resulting from interaction between measuring devices. An overall picture of the flow was then synthesized from data obtained from repeated experiments.

Table 1 Experimental Conditions.

Experiment Facility A		
θ (°)	B_0(cm/s^2)	q_0(cm^2/s)
5.00	2.45	3.39 5.01
	4.90	3.37 5.07
	9.80	3.38 5.09
5.71	20.58	9.00
8.13	20.58	9.00
10.00	2.45	3.34 5.00
	4.90	3.31 4.98
	9.80	3.34 4.97
20.00	2.45	2.16 4.30
	4.90	2.15 4.32
	9.80	2.16 4.38
Experiment Facility B		
θ (°)	B_0(cm/s^2)	q_0(cm^2/s)
45.00	4.90	1.03 2.03
	9.80	1.02 2.02
	19.60	1.02 2.02
60.00	4.90	0.62 1.01
	9.80	0.62 1.01
	19.60	0.62 1.01
90.00	4.90	0.63 1.01
	9.80	0.63 1.01
	19.60	0.64 1.01

EXPERIMENTAL RESULTS

When an inclined starting plume is set up by a continuous release of a constant buoyancy flux, the propagation speed of the front part changes gradually until it becomes about constant in the equilibrium state. Such a condition is achieved by the force balance between gravitational force down the incline and the resistance force due to form and entrainment drag, as was

demonstrated numerically by Akiyama *et al.*(1). Flow characteristics to be described below were quantified using experimental data in the equilibrium state, which was determined by the constancy of the front propagation speed.

Observation of the Flow

An example of strip-charts, essentially showing the variation of velocity within the current with elapsed time, is presented in Fig. 2. Therein, experimental conditions as well as the measurement position are also included. Fig. 2 reveals that the flow is turbulent throughout the current and the mean velocity of the front part is nearly constant, except near the foremost and tail part of the front structure. The reduction of velocity indicates that a large eddy created on the upper interface of the front penetrates even closer to the bottom boundary. Such velocity reduction clearly distinguishes the front part from the body part.

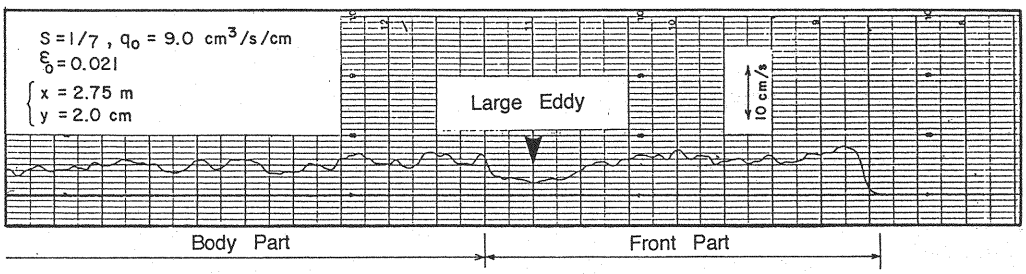

Fig.2 Example of Strip-chart.

Using experimental data for the case of θ=5.17° and 8.13° , similarity of velocity and density profiles are tested in Figs. 3a and 3b, respectively. In the body part, the similarity of the velocity and density profiles is clearly seen, whereas, in spite of scatter, a general trend toward an approximate similarity of the profiles can be identified even in the front part. Therein, δ is defined such that $u=1/2u_{max}$ at $y=\delta$.

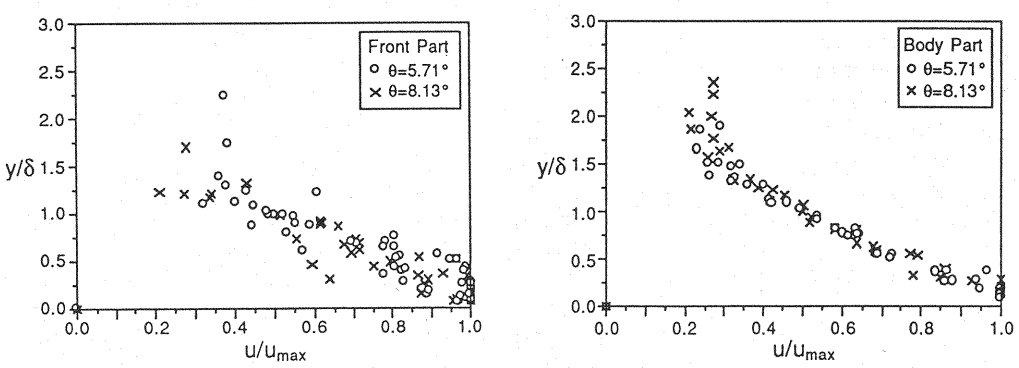

(a) Front Part (b) Body Part

Fig.3a Similarity Profile (Velocity).

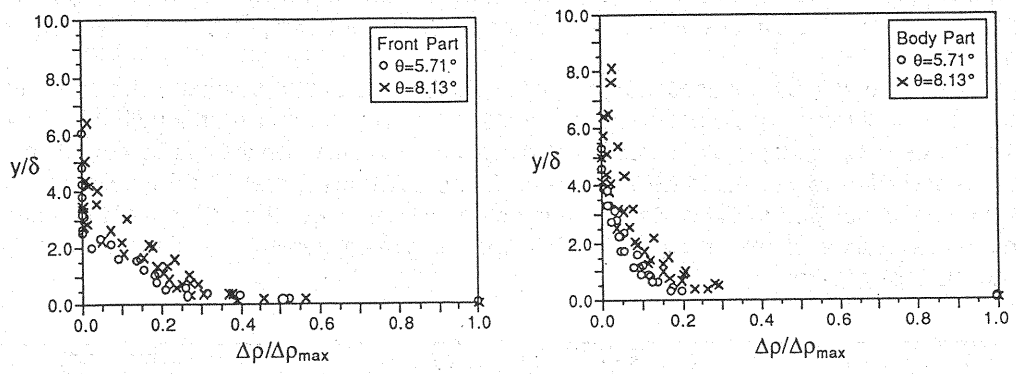

(a) Front Part (b) Body Part

Fig.3b Similarity Profile (Density).

Dimensionless Front Propagation Speed (U_{fe}^*)

The front propagation speed U_{fe} in the equilibrium state is controlled by the layer averaged buoyancy force B_f and the maximum flow height h_f of the front part. From dimensional analysis or simple analytical considerations based on a balance of forces, U_{fe} is expressed as

$$U_{fe} = K(B_f h_f)^{1/2} \qquad (1)$$

This form of U_{fe}, which implies that an overall Richardson number based on properties of the front part is constant with x, has been used by various investigators. Middleton(14), for example, proposed that the value of the coefficient K is about 0.75 for the bottom slope angle less than a few degrees, whereas, for the horizontal bottom, K=1.1 was proposed by Kranenburg(11). The value of K is, in general, considered to be functions of slope angles.

Alternatively, the volume inflow rate per unit width q_0, the density of the ambient water ρ_a, the density of the dense water ρ, the angle of the slope θ, and the kinematic viscosity of the flow ν are selected as independent variables. Dimensional considerations yield the following relationship:

$$\phi\left(U_{fe}^*,\ R_e,\ \theta\right) = 0 \qquad (2)$$

where U_{fe}^* is the dimensionless front propagation and R_e is the Reynolds number defined, respectively, by Eqs. 3 and 4.

$$U_{fe}^* = \frac{U_{fe}}{(B_0 q_0)^{1/3}} \qquad (3)\ ; \qquad R_e = \frac{(B_0 q_0)^{1/3} h_f}{\nu} \qquad (4)$$

Since Eq. 3 is expressed in terms of known properties, U_{fe}^* is considered to be more significant than U_{fe} given by Eq.1 for describing the front propagation speed. The importance of the parameter U_{fe}^* has been recognized by Wood(17) and Britter & Linden(6). In particular, Britter & Linden found experimentally that on slopes from 5° to 90° , U_{fe}^* is only a weak function of

slope angle θ and approximately constant with a weak maximum at 20~40° . Consequently, it is proposed that the dimensionless front propagation speed is approximately given by U_{fe}^{*} =1.5±0.2.

The case of θ=60° is used to highlight the significance of the parameter U_{fe}^{*}. The values of U_{fe} under different inflow conditions were plotted against the intrusion length x in Fig.4a. The values of U_{fe}^{*} become almost constant irrespective of inflow conditions (Fig.4b), while the values of U_{fe} differ substantially depending on inflow conditions (Fig.4a). The Reynolds number R_e for fully developed inclined starting plumes on inclines larger than 5° are of the order of several thousands, so that no significant R_e dependence is observed. U_{fe}^{*} is, therefore, only a function of slope angle.

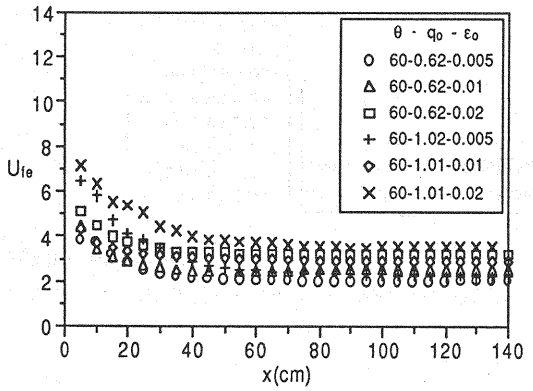

Fig.4a Variation of U_{fe}(in cm/s) with x(θ=60°).

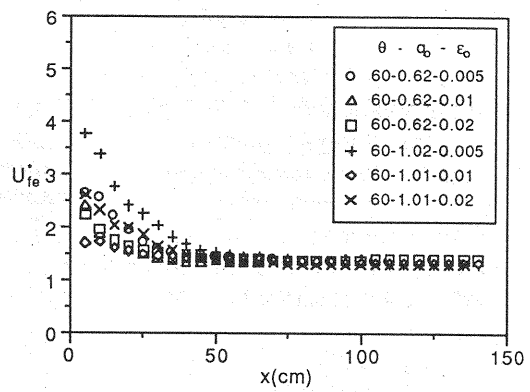

Fig.4b Variation of U_{fe}^{*} with x(θ=60°).

The average value of U_{fe}^{*} at a given bottom slope angle was determined by taking an ensemble mean of U_{fe}^{*}. One case of frequency diagram(θ=5°) is presented in Fig. 5. In Fig. 6, the dependence of U_{fe}^{*} upon θ is examined and compared with Britter & Linden's results. The present data shows less strong and less systematic dependence of U_{fe}^{*} on θ than Britter & Linden's results. U_{fe}^{*} may be approximately given as follows :

$$U_{fe}^{*} = 1.34 \pm 0.03 \qquad (5)$$

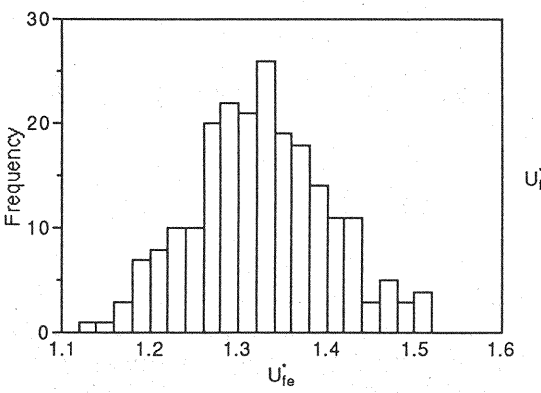

Fig.5 Frequency Diagram of U_{fe}^{*} (θ=5°).

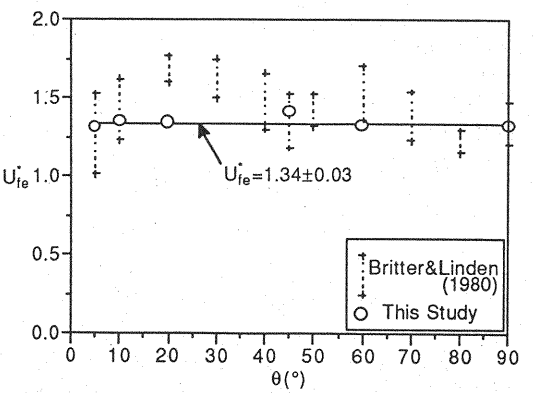

Fig.6 Dependence of U_{fe}^{*} on θ.

Geometry of the Front

Owing to the occurrence of intermittent large-breaking eddies being left behind the front part, the determination of the front geometry is difficult for small θ, perhaps, $\theta \leq 10°$. However, a careful inspection of the present experimental data reveals that for a given bottom slope the geometry of the front holds an approximately similar shape along its path, provided that localized instantaneous protrusions are averaged out. A few cases of dimensionless front shape are depicted in Fig.7. Here, the vertical and horizontal coordinates are normalized by the maximum height h_f and the length L of the front. The geometry of the front appears to be independent of inflow conditions, but dependent on bottom slope angles. The shape of the front part may be expressed as a quarter-ellipse when θ is less than 10° and a half-ellipse when θ=10~90° .

It is impossible to express the geometry of the front in terms of a simple function for a bottom slope angle range of 5° to 90° . The volume correction factor S(θ) and the length-to-height ratio f(θ) are introduced as follows :

$$S(\theta) = \frac{A}{h_f L} \qquad (6)$$

$$f(\theta) = \frac{h_f}{L} \qquad (7)$$

where A=volume of the front part per unit width.

Fig.8 shows that S(θ) is a very weak function of θ. Excluding data for bottom slope angles of less than 10° , S(θ) may be approximated as follows :

$$S(\theta) = 0.785 \pm 0.017 \qquad (8)$$

S(θ)=0.785 is the area of half-ellipse(=π/4), which is illustrated by a solid line in Fig.8.

An empirical relationship for f(θ) was proposed by Britter & Linden(6), based on their own experimental data as well as that

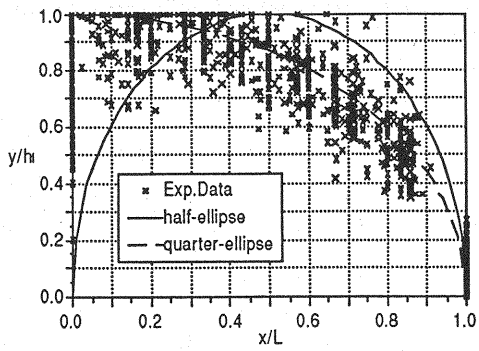

(a) θ = 5°

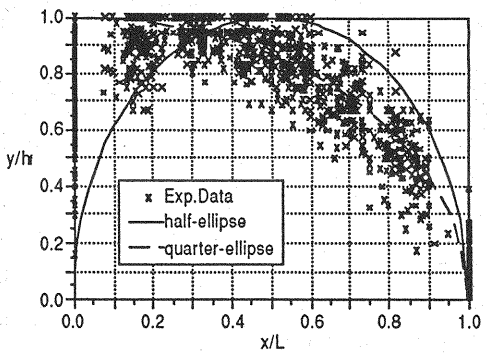

(b) θ = 10°

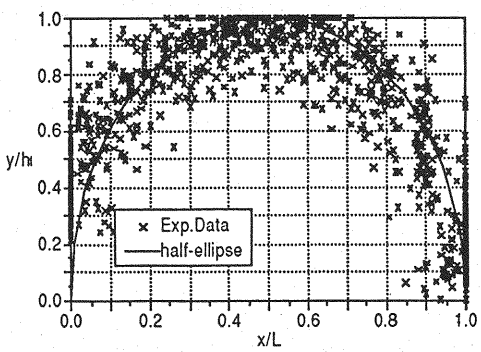

(c) θ = 45°

Fig.7 Dimensionless Front Shape.

of Hopfinger & Tochon-Danguy(8) and Wood(17). A fitted empirical equation, $f(\theta)=0.00275\theta+0.24$ for $\theta=5\sim90°$, may be deduced from their results. However, $f(\theta)$-relationship obtained using a large number of the present data shows that $f(\theta)$ is more strongly dependent on θ than that of Britter & Linden. An example of frequency diagrams($\theta=20°$) is presented in Fig.9 and the dependence of $f(\theta)$ on θ is examined in Fig.10. The following empirical relationship may adequately describe $f(\theta)$;

$$f(\theta) = 0.0053\theta + 0.2 \qquad (9)$$

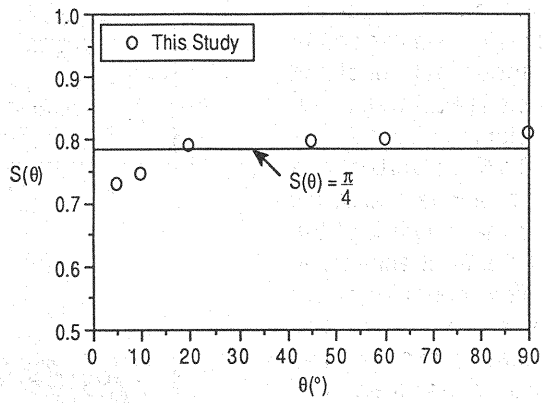

Fig.8 Dependence of $S(\theta)$ on θ.

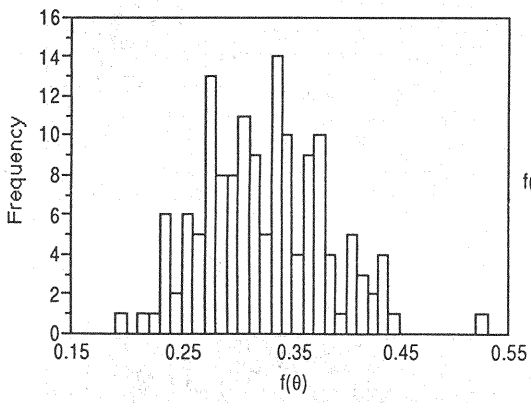

Fig.9 Frequency Diagram of $f(\theta)(\theta=20°)$.

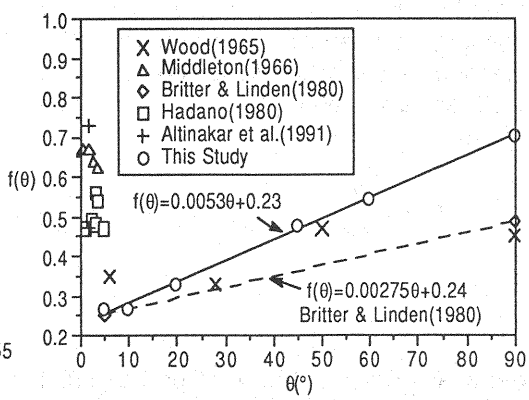

Fig.10 Dependence of $f(\theta)$ on θ.

Growth Rate of Maximum Front Height (dh_f/dx) and the Body Part (dh/dx)

Variation of flow height with distance from the initial point shows that the height h of the body part, as well as the height h_f of the front part, increases about linearly in the downstream direction. The spatial growth rate dh_f/dx of the front is substantially larger in magnitude than dh/dx of the body part. In the front part, the head volume increases by the net flux resulting from three fluxes : the intense entrainment caused by large eddy motion, the inflow of the dense fluid from the body part into the front part, and the intermittent loss of front volume behind the front. Fig.11 shows the dependence of dh_f/dx and dh/dx on θ. Therein, the results of this study are supplemented with the results of Altinakar *et al.*, Britter & Linden, and others.

A fitted empirical equation given by Eq.10 agrees fairly well even with the data of Altinakar *et al.*, which were obtained for bottom slope angles of less than 5° .

Britter & Linden(6) found experimentally that dh_f/dx is dependent linearly on a bed slope angle and is expressed as $dh_f/dx=0.004\theta$ for $\theta=5\sim90°$. Similar results were reported by Luthi(12) for the range of $\theta=0\sim5°$. On the other hand, the motion of the body part is considered to be analogous to that of a continuous inclined plume, which yields $dh/dx=0.00095(\theta+5)$ according to Ellison & Turner(10). The present experimental results can be fitted by the following empirical results :

$$\frac{dh_f}{dx} = 0.0037\theta \tag{10}$$

$$\frac{dh}{dx} = 0.0009\,(\theta + 5) \tag{11}$$

It may be concluded from Eqs.10 and 11 that not only the magnitude of spatial growth rate dh/dx of the body part is identical to that of the continuous inclined plume investigated by Ellison & Turner, but also that Britter & Linden's results for dh_f/dx is surprisingly consistent with the present results, even though they were based on a limited amount of experimental data. This may be because, unlike other front flow properties, the determination of dh_f/dx does essentially involve a large volume of data; the value of dh_f/dx is determined from the envelope of the family of the front part.

Using Eqs.10 and 11, the dependence of the flow thickness ratio h_f/h on θ is examined. Integrating Eqs.10 and 11 with respect to x with initial conditions (h_{f0}, h_0), and allowing h_{f0}/x and h_0/x to be negligibly small at large x, Eq.12 may be obtained :

$$\frac{h}{h_f} = \frac{\theta + 5}{4.1\,\theta} \tag{12}$$

The present and the existing data by Michon *et al.*(13), Middleton(14), and Wood(17) are plotted against θ in Fig.12. It shows that h_f/h increases sharply for smaller values of θ; i.e., less than about 10° . As θ increases, the increment in h_f/h gradually decreases and for θ greater than 40° , h_f/h becomes more or less constant with increasing θ.

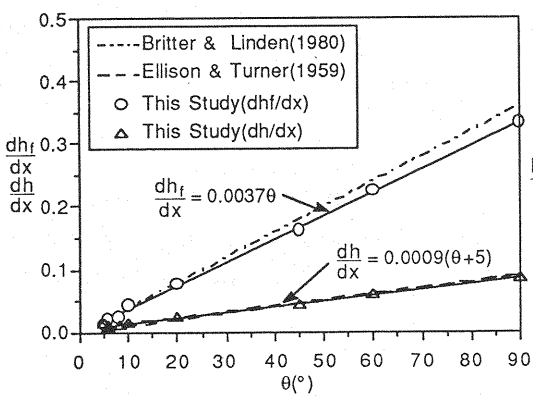

Fig.11 Dependence of dh/dx and dh_f/dx on θ.

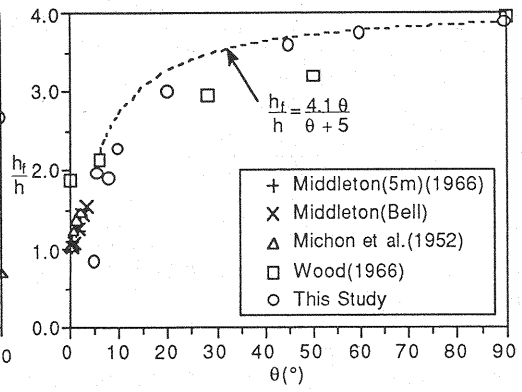

Fig.12 Dependence of h/h_f on θ.

Velocity Ratio(U_{fe}/U)

For very mild bottom slope angles, the velocity ratio U_{fe}/U has been examined by Middleton(14), assuming conservation of volume between the body part and the front part ($U_{fe}/U=h/h_f$). However, for moderately mild and steep bottom slope angles (θ=5~90°) intensive mixing takes place in the front part. Consequently, U_{fe}/U cannot be estimated through the simple relationship given above. The following basic analysis has been carried out to find the relationship between U_{fe} and U. Considering a stream line between the stagnation point at the foremost point of the front part and an equilibrium state in the body part, Bernoulli's equation with Boussinesq's approximation under the assumption that the energy loss is equal to change of potential energy leads to

$$U_{fe}^2 = (u_b - U_{fe})^2 + 2B\beta_2 h\cos\theta \tag{13}$$

where β_2=profile constant, u_b=velocity on the considered stream line.

Defining the overall Richardson number R_i of the body part as

$$R_i = \frac{Bh\cos\theta}{U^2} \tag{14}$$

and assuming that the body part is in the equilibrium(normal) condition, characterized by an invariant R_i-number in the flow direction, the velocity ratio U_{fe}/U is expressed as

$$\frac{U_{fe}}{U} = \frac{1}{2}\alpha\left(1+\frac{2\beta_2 R_{in}}{\alpha^2}\right) \tag{15}$$

where R_{in} is the overall Richardson number in the normal condition, α is the ratio of the velocity u_b to the mean velocity U in the body part, namely, $\alpha=u_b/U$.

R_{in} in Eq.15 can be obtained from dR_i/dx-equation, which is one of the governing equations for describing a continuous inclined plume (see Ellison & Turner[10], Akiyama & Stefan[3]);

$$\frac{dR_i}{dx} = \frac{3R_i}{h}\left(\frac{(1+\beta_1 R_i/2)E_e - \beta_2 R_i\tan\theta + f_b}{1-\beta_1 R_i}\right) \tag{16}$$

where E_e=entrainment coefficient in the body flow($=v_e/U$), v_e=entrainment velocity, f_b=friction coefficient, and β_1=profile constant.

Setting $dR_i/dx=0$ or $R_i=R_{in}$ in Eq.16, R_{in} is obtained as

$$R_{in} = \frac{E_e + f_b}{\beta_2\tan\theta - \beta_1 E_e/2} \tag{17}$$

The empirical entrainment coefficient in the form of Eq.18, which was proposed by Turner(15), is presumed to be valid for the body part; applicability of Eq.18 to the body part is examined in the next section.

$$E_e = \frac{0.08 - 0.1R_i}{1+5R_i} \tag{18}$$

Setting $R_i=R_{in}$ in Eq.18 and then eliminating E_e from Eqs.17 and 18, R_{in} can be obtained as

follows :

$$R_{in} = \frac{-A_2 + \sqrt{A_2^2 - 4A_1A_3}}{2A_1} \tag{19}$$

where $A_1=0.05\beta_1+5\beta_2\tan\theta$; $A_2=0.1-0.04\beta_1+\beta_2\tan\theta-5f_b$; $A_3=-0.08-f_b$.

With the use of $f_b=0.01$, $\beta_1=0.25$, and $\beta_2=0.75$, Eq.19 is calculated for different α-values. The values of $\beta_1=0.25$ and $\beta_2=0.75$ are selected based on the average of β_1-, and β_2-values, which typically vary $\beta_1=0.2\sim0.3$ and $\beta_2=0.6\sim0.9$ according to Ellison & Turner(10). It is found that $\alpha=0.8$ yields reasonable agreement between experimental and calculated results. U_{fe}/U decreases gradually to attain a constant value as θ increases as shown in Fig.13. The velocity ratio becomes a function of θ only, and the following semi-empirical relationship can be obtained :

$$\frac{U_{fe}}{U} = 0.4 - \frac{0.04 + 0.75\tan\theta - \sqrt{0.5625\tan^2\theta + 1.41\tan\theta + 0.0061}}{0.0267 + 8\tan\theta} \tag{20}$$

Eq.20 indicates that at a given slope angle the front velocity is a constant fraction of the body part velocity behind the front. This is consistent with the experimental observations(Britter & Linden[6], Hopfinger & Tochon-Danguy[8]) and the numerical results(Akiyama *et al.*[1]).

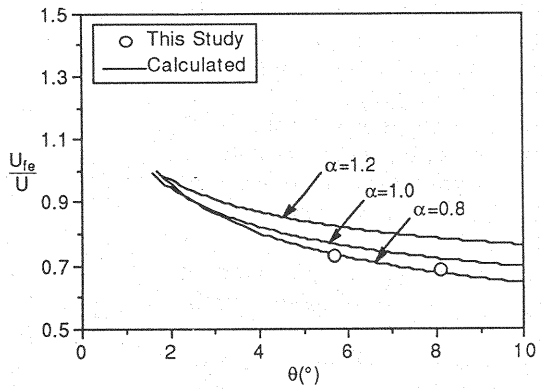

Fig.13 Relationship Between U_{fe}/U and θ.

Entrainment Coefficient for the Body Part(E_e) and for the Front Part(E_d)

First, the entrainment coefficient E_e of the body part is examined. The conservation of volume allows E_e to be given by

$$E_e = \frac{(1/U)d(Uh)}{dx} \tag{21}$$

The difference in entrainment characteristics between the body part of inclined starting plumes and continuous inclined plumes may be due only to the re-entrainment of the fluid left behind the front part, caused by a series of intermittent large eddies breaking away into the body part. However, since the density difference of the fluid left behind the front part is too small to alter entrainment characteristics significantly, it is plausible to assume that entrainment

characteristics in the body part may be analogous to those of a continuous inclined plume.

Since in the equilibrium state the layer averaged flow velocity U becomes invariant with x as immediately seen from the definition of R_i, Eq.21 reduces to

$$E_e = \frac{dh}{dx} \tag{22}$$

As has been shown in Fig.11, the obtained values of dh/dx are consistent with those for continuous inclined plumes. The difference between the two results is merely due to an error associated with experiment. This fact highlights that a fundamental similarity in entrainment characteristics exists between continuous inclined plumes and the body part of inclined starting plumes, implying $E_e \sim 0.00095(\theta+5)$. It also indicates that the body part is mostly free from the front part in the case of $\theta=5\sim90°$.

The empirical entrainment coefficient in the form of Eq.18 is compared with the present experimental data in Fig.14. R_{in} estimated from Eq.19 is denoted by the open square symbol and R_i calculated from velocity and density measurements, i.e. ,the case of $\theta=5.71°$ and $8.13°$,is denoted by the open circle symbol. Therein, U, B and h are determined from the method of moments. It shows that Eq.18 agrees reasonably with the present experimental results. It must be noted that in normal conditions, the value of E_e is uniquely related to the bottom slope angle and hence the range of data shown in Fig.14 is rather narrow.

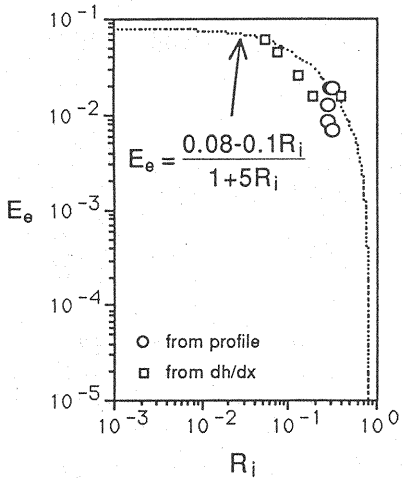

Fig.14 Entrainment Coefficient E_e vs. R_i-number.

Next, the entrainment coefficient E_d of the front part is quantified. Intense mixing between the ambient and front fluid occurs in the front part. Since the front is mainly controling the flow, mixing at the front is more important than in the body part. The instantaneous volume balance in the front part is caused by the amount of direct entrainment q_e, the amount of influx q_i from the body part into the front part, and the amount of efflux q_o from the front part into the mixed layer resulting from the dense fluid being mixed out of the front part by the less dense fluid. That is,

$$\frac{dA}{dt} = q_i + q_e - q_o \tag{23}$$

However, it is impossible to quantify an instantaneous influx q_i experimentally although the determination of $\Delta A/\Delta t$ is possible from a visualized front shape. ΔA is difference of the front volume per unit width in a small elapsed time Δt. Therefore, the amount of the averaged net entrained flux $\bar{q}_e$, which is defined as $\overline{(q_e - q_o)}$, is considered. The notation "$\bar{\ }$" means the averaged quantity. $\bar{q}_e$ is expressed as

$$\bar{q}_e = \frac{\overline{\Delta A}}{\Delta t} - \bar{q}_i \tag{24}$$

Assuming that the body part is in the fully developed state, $\bar{q}_i$, which is expressed by

Eq.25, is approximately estimated by the method described below.

$$\bar{q}_l = \overline{h(U - U_f)} \tag{25}$$

The instantaneous front propagation speed U_{fe} under a given condition fluctuates along the flow path, but the average front propagation speed $\bar{U}_{fe}$ is about constant in the fully developed state. Likewise, the body part flows down an incline with constant speed $\bar{U}$ in the equilibrium state. It means that in the fully developed state the average flux $\bar{q}_l$ increases linearly in the flow direction.
Eq.25 can be rewritten as

$$\bar{q}_l = \bar{q}\left[1 - \left(\frac{\overline{U_{fe}}}{\bar{U}}\right)\left(\frac{\overline{U_f}}{\overline{U_{fe}}}\right)\right] \tag{26}$$

where $\overline{U_{fe}/U}$ can be calculated by Eq.20 and $\overline{U_f/U_{fe}}$ is calculated from the following equation:

$$\frac{\overline{U_{fe}}}{U_f} = 1 + \frac{1}{f(\theta)}\frac{dh_f}{dx} \tag{27}$$

$\bar{q}$ is the discharge per unit width in the body part(=$\overline{Uh}$) and is determined by

$$\bar{q} = q_0 + E_e \bar{U} x \tag{28}$$

For the fully developed state $\bar{U}$ is constant in the flow direction and is given by

$$\bar{U} = \left(\frac{B_0 q_0}{R_{in}}\right)^{1/3} \tag{29}$$

where $B_0 q_0$ is the initial buoyancy flux and is conserved throughout in the body flow, and R_{in} is given by Eq.19 .

Upon estimation of the amount of $\bar{q}_e$, the entrainment coefficient E_d for the front part, defined by Eq.30, can be determined.

$$E_d = \frac{\bar{q}_e}{L U_{fe}} \tag{30}$$

The E_d-function defined above is based on L, a length scale and U_{fe}, a velocity scale. Conversion of the E_d-function into the entrainment function based on the mass-centre velocity U_f is possible through Eq.27. Likewise, conversion of the E_d-function into the entrainment function based on the front maximum height h_f is possible through Eq.7. Furthermore, conversion of the E_d-function into the entrainment function based on the front circumference C is possible through the following geometrical relationship:

$$\frac{C}{L} = \left(\frac{\pi}{2^{3/2}}\right)\sqrt{4f(\theta)^2 + 1} \tag{31}$$

The occurrence of intermittent breaking eddies makes the front grow and decay in alternate sequence. This phenomenon causes variations of E_d-values in a manner similar to other flow characteristics. One case of frequency diagrams is shown in Fig.15. The average E_d-values are determined by taking the ensemble mean and regress against bottom slope angles. As seen from Fig.16, E_d increases about linearly with increasing slope angles. The following empirical E_d-function can be obtained :

$$E_d(\theta) = 0.0045\theta \qquad (32)$$

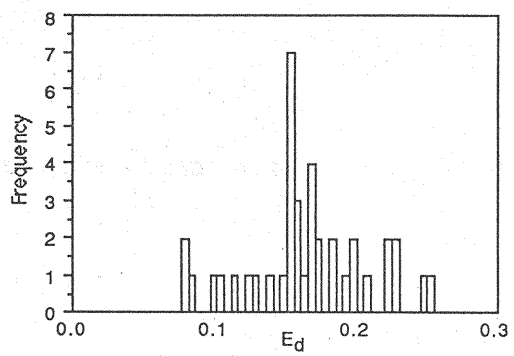

Fig.15 Frequency Diagram of $E_d(\theta=45^\circ)$.

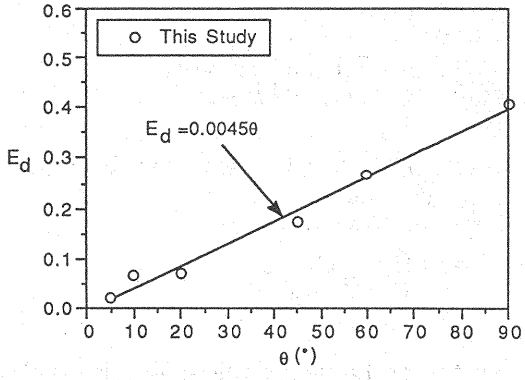

Fig.16 Entrainment Coefficient E_d vs. θ.

CONCLUSION

Major gross flow characteristics of a miscible inclined starting plume are experimentally quantified through a series of experimental studies. It was found that the dimensionless front propagation speed U_{fe}^*, the volume correction factor S, the front aspect ratio f, the spatial growth rate of the front part dh_f/dx and the body part dh/dx, the layer thickness ratio h/h_f, the velocity ratio U_{fe}/U, and the entrainment function for the front part E_d and the body part E_e are all functions of bottom slope angle θ when the flow is turbulent (θ=5~90°). The empirical relationships, established based on the large volume of present experimental data, are sufficiently accurate. Therefore, they can be used for constructing a new analytical or a hybrid model for an on-site simulation, examining the quality of experimental data, and predicting the behaviors of inclined starting plumes under ideal situations.

ACKNOWLEDGEMENT

This study was supported by the Grant-in-Aid for Science Research (C) of the ministry of Education and Culture, Japan under the Grant NO.6650568.

REFERENCES

1. Akiyama,J., W.Wang and M.Ura : Numerical model of unsteady inclined plumes, Proceedings of Hydraulic Engineering, JSCE, Vol.35, pp.167-172, 1991(in Japanese).
2. Akiyama,J. and M.Ura : Characteristics of gravity currents traveling downslope, Proceedings

of the Int'l Sympo. on Environmental Hydraulics, Hong Kong, pp.565-570, 1991.
3. Akiyama,J. and H.Stefan : Turbidity current with erosion and deposition, Journal of Hydraulic Engineering, ASCE, Vol.111, No.12, pp.1473-1496, 1985.
4. Akiyama,J. : Inclined plume and thermal, Journal of Hydroscience and Hydraulic Engineering, Special Issues, Research and Practice of Hydraulic Engineering in Japan, No.S1-1 Hydraulics, Chapter 3.3, pp.84-91, 1993.
5. Altinakar,M.S., W.H.Graf and E.J.Hopfinger : Weakly depositing turbidity current on a small slope, Journal of Hydraulic Research, Vol.28, No.1, pp.55-80, 1990.
6. Britter,R.E. and P.F.Linden : The motion of the front of a gravity current traveling down an incline, Journal of Fluid Mechanics, Vol.99, pp.531-543, 1980.
7. Hadano,K. : Study on the front of a turbidity current, Memoirs of the Faculty of Eng., Kyushu University, Vol.41,4, pp.307-317, 1981(in Japanese).
8. Hopfinger,E.J. and J.C.Tochon-Danguy : A model study of powder snow avalanches, Journal of Glaciology, Vol.19,8, pp.343-356, 1977.
9. Fukuoka,S., K.Mizumura and T.Kanoh : Fundamental study on the dynamics of the head of gravity currents, Proceedings of JSCE, Vol.274, pp.41-55, 1978(in Japanese).
10. Ellison,T.H. and J.S.Turner : Turbulent entrainment in stratified flow, Journal of Fluid Mechanics, Vol.6, pp.423-448,1959.
11. Kranenburg,C. : Internal fronts in two-layer flow, Journal of the Hydraulic Division, technical note,ASCE, Vol.104, HY10, pp.1449-1453, 1979.
12. Luthi,S. : Some new aspects of two-dimensional turbidity currents, Sedimentology, Vol.28, pp.97-105, 1980.
13. Michon,S., J.Goddet and R.Bonnefille : Etude theorique et experimentale des courants de densite, Tomel et 2, Laboratoire National d'Hydraulique, Chatou, France, 1955.
14. Middleton,G.V. : Experiments on density and turbidity currents, 1.motion of the head, Canadian Journal of Earth Science, Vol.3, pp.523-546, 1966.
15. Turner,J.S. : Turbulent entrainment: the development of the entrainment assumption, and its application to geophysical flows, Journal of Fluid Mechanics, Vol.173, pp.431-471, 1986.
16. Simpson,J.E. and R.E.Britter : The dynamics of the head of a gravity current advancing over a horizontal surface, Journal of Fluid Mechanics, Vol.94, pp.477-495, 1979.
17. Wood,I.R. : Studies in unsteady self-preserving turbulent flows, The University of New South Wales, Water Research Laboratory Report, No.81, 1966.

Appendix - NOTATIONS

The following symbols are used in this paper:

A = cross-sectional area of the front part;

B = layer averaged buoyancy force ;

C = circumference of the front part ;

E_e = entrainment coefficient of the body part ;

E_d = entrainment coefficient of the front part ;

$f(\theta)$ = length-to-height ratio of the front part ;

g = acceleration due to gravity ;

h = flow thickness ;

L = length of the front part ;

q_e = amount of entrained fluid ;

q_f = buoyancy flux ;

q_i = amount of influx from the body to the front part ;

q_o = amount of efflux from the front to the mixed layer

R_i = overall Richardson number ;

$S(\theta)$ = volume correction factor of the front part ; and

U = layer averaged flow velocity .

Subscript

a = refers to ambient fluid ;

f = refers to the property of the front part ;

fe = refers to the properties of the foremost point of the front part ; and

o = refers to the property at upstream boundary .

Superscript

$*$ = refers to dimensionless property .

Greek

α = velocity ratio ;

β = profile constant ;

ε = relative density difference ;

ρ = density of fluid ;

θ = bottom slope angle ; and

ν = kinematic viscosity of fluid .